




Encapsulated core–sheath carbon nanotube–graphene/polyurethane composite fiber for highly stable, stretchable, and sensitive strain sensor

Yiman Xu¹, Xiaoxu Xie¹, Hong Huang^{2,*}, Yan Wang^{1,*} , Junrong Yu¹, and Zuming Hu¹

¹ Shanghai Collaborative Innovation Center for High Performance Fiber Composites, State Key Laboratory for Modification of Chemical Fibers and Polymer Materials, College of Material Science and Engineering, Donghua University, Shanghai 201620, People's Republic of China

² College of Biological, Chemical Sciences and Engineering, Jiaying University, Jiaying 314001, People's Republic of China

Received: 6 August 2020

Accepted: 25 September 2020

Published online:

6 October 2020

© Springer Science+Business Media, LLC, part of Springer Nature 2020

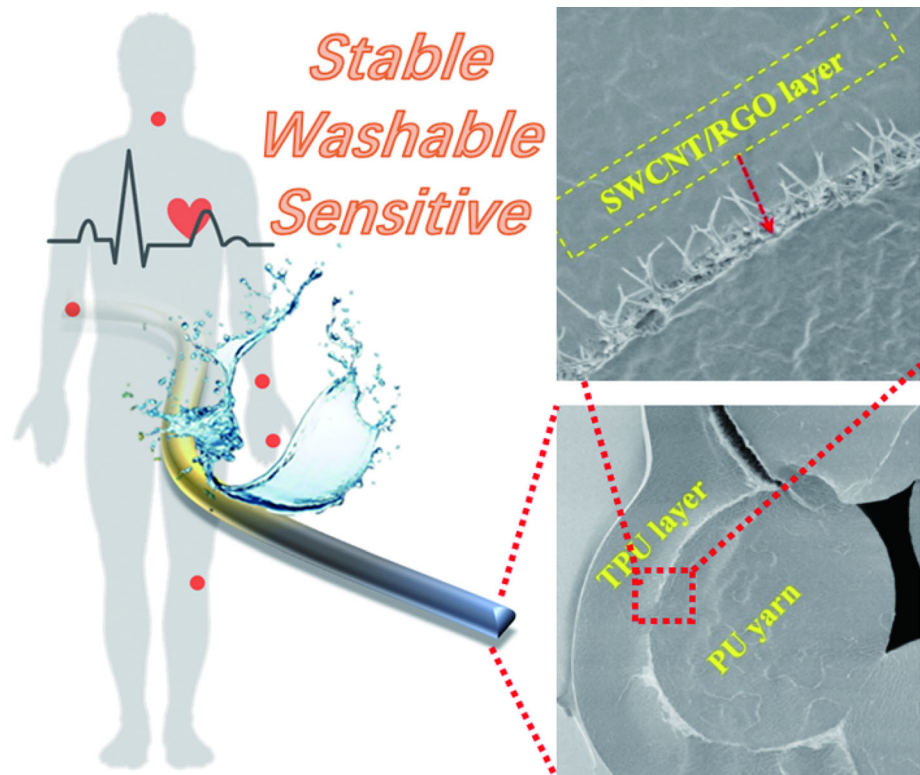
ABSTRACT

Stretchable and sensitive fiber-shaped strain sensor with stable sensing performance is highly desirable for wearable electronics. However, it is still a challenge to simply and economically fabricate such strain sensors in large scale for practical applications. Herein, we report a strain sensor based on a thermoplastic polyurethane (TPU) layer encapsulated core–sheath single-walled carbon nanotube (SWCNT)-reduced graphene oxide (RGO)/PU composite fiber through a dip-coating process. The synergistic effect between SWCNT and RGO contributes to the formation of a highly sensitive and conductive layer on elastic PU core, while the outmost TPU layer protects the conductive layer against abrasion or delamination. The results demonstrate that the fiber sensor with 50 wt% RGO in the conductive layer simultaneously exhibits a wide sensing range of 465%, a high gauge factor (GF) up to 114.7, and good cyclic stability for more than 1000 stretching cycles. Importantly, the fiber sensor shows high stability with little change in conductivity even by harsh treatment in ultrasonic bath for 250 min. The applications of our fiber sensor in monitoring human motions like elbow bending, phonation, pulse, and underwater sensing are also demonstrated. The reported fiber strain sensor provides a good candidate for next-generation intelligent wearable devices.

Handling Editor: Kevin Jones.

Address correspondence to E-mail: huangho17@163.com; wy@dhu.edu.cn

GRAPHIC ABSTRACT



Introduction

Next-generation intelligent wearable electronic devices put forward increasingly stringent demands, such as small size, lightweight, flexible, and skin-mountable [1, 2]. Therefore, flexible batteries [3, 4], supercapacitors [5–7], strain sensors [8, 9], and other wearable electronic devices with high flexibility, which can be folded into any shape and woven or sewn onto clothes, have recently attracted tremendous attention. Among these devices, soft and stretchable strain sensors are widely studied, especially resistive sensors with simple structures that are easy to collect signals and convert stress/strain into resistance changes. To date, combining conductive nanomaterials with a flexible and stretchable matrix is the main strategy for obtaining such strain sensors. Among all the conductive fillers, carbon nanomaterials, including carbon nanotube (CNT) [10, 11], graphene [12–15], and carbon

black (CB) [16, 17], are probably the most frequently used fillers to fabricate strain sensors. It is recently reported that the combination of fillers with different dimensions is more efficient in the construction of homogeneous conductive networks than single filler, because the synergistic effect between different fillers could effectively prevent aggregations of nanosized fillers [18–20]. However, few works have exploited the synergistic effect of different carbon nanomaterials for sensor applications. By physical blending of CNT and RGO with polyurethane, Liu et al. obtained a strain sensor with working range of 30% and GF of 152.9 [21]. Zheng et al. fabricated a strain sensor with carbon nanofiber (CNF) and CB as fillers in elastomer, and showed a high strain range of 300% and GF of 13.1 [22]. Likewise, Yang et al. reported a strain sensor with a good stretchability of 700% and maximum GF of 182 by incorporating carbon fiber and CB into a rubber matrix [23]. Shi et al. reported a strain sensor with high conductivity and GF by hybridizing graphene into CNT

network, but the working range was limited to 20% due to the lack of elastic component [24]. Other strain sensors based on synergistic effect of carbon nanomaterials have also been reported by various approaches [25–28], but rare works have achieved high stability, stretchability, and sensitivity.

At present, planar structures are commonly used to fabricate strain sensors [29–32]. However, these structures limit their applications in flexible textiles or complex nonplanar substrates, which has largely hindered their use in flexible and sensitive strain sensors. To this end, high-performance fibrous strain sensors have promising application prospects due to their high flexibility, stretchability, and rebound elasticity [33–36]. Techniques like doping or coating conductive materials were reported to manufacture fibrous sensing devices [37–40]. For example, by incorporating CNT into cotton roving, a sensor based on CNT/cotton/spandex composite yarn was manufactured and showed high performance in wearable electronic device [41]. Conductive cotton [14, 42] or polyester fabrics [43] prepared by simply coating with RGO have also been reported for wearable strain sensors. Nevertheless, by using the doping or coating technique, the conductive layers are prone to flake off due to repeated washing and long-term use. Moreover, the conductive layers of these sensors are often exposed, which may lead to a short circuit, thus hindering their practical applications. Therefore, it is necessary to develop a practical, cost-effective, and scalable method to fabricate sensitive, highly stretchable, and durable fiber strain sensors.

We have recently reported a spirally layered strain sensor based on SWCNT-RGO/PU composite yarn [44]. The synergistic effect of SWCNT-RGO in the conductive layer and the special structure enables the strain sensor a combined performance of high strength, conductivity, sensitivity, and durability. However, the complex manufacturing process limits its large-area and facile production. Therefore, here we report a new stable and sensitive strain sensor based on a core–sheath SWCNT-RGO/PU composite fiber encapsulated in a protective TPU layer by a simple and scalable dip-coating method. We used PU multifilament as an elastic scaffold and applied SWCNT-RGO mixed network as conductive layer. The SWCNT-RGO/PU core–sheath fiber was then embedded into a stretchable TPU protective layer to prevent the conductive layer from wearing or delaminating. The synergistic effect of SWCNT and RGO endowed our

strain sensor with good sensing performance. The results show that the sensing range of our sensor with 50 wt% RGO in conductive layer can be up to 465% with a high GF of 114.7. Increasing the RGO content results in even higher GF at the same strain. Importantly, our sensor shows high stability against rigorous ultrasonic washing because of the encapsulated structure. On the basis of these advantages, the fiber strain sensor can be applied for long-term use in monitoring human motions like phonation, elbow bending, and even pulse. The ability of our sensor for underwater sensing is also demonstrated. The reported technology is expected to provide a new way to next-generation intelligent wearable technology.

Experimental section

Materials

Graphite powder (300 μm) was provided by Qingdao Chenyang Graphite Co., Ltd. PU multifilament (140 D) was provided by LDZ New Aoshen Soandex Co., Ltd. Potassium permanganate (KMnO_4) was purchased from Jiangsu Yonghua Fine Chemical Co., Ltd. Concentrated sulfuric acid, sodium nitrate (NaNO_3), hydrogen peroxide (H_2O_2 , 30%), and hydrazine hydrate were purchased from Sinopharm Pharmaceutical Co., Ltd. Thermoplastic polyurethane (TPU, Elastollan 1180A) was purchased from BASF Co., Ltd. Single-walled carbon nanotubes (SWCNTs) were obtained from Chengdu Organic Chemicals Co., Ltd., Chinese Academy of Science. Poly(3,4-ethylenedioxythiophene) polystyrene sulfonate (PEDOT:PSS, Clevios PH1000) was obtained from Heraeus GmbH. Ammonia water and *N,N*-dimethylformamide (DMF) were purchased from Shanghai Lingfeng Chemical Reagent Co., Ltd.

Preparation of SWCNT-RGO dispersion

RGO was prepared according to our previous work with PEDOT:PSS as stabilizing agent, and the preparation process and characterizations of RGO can be found in our previous paper [44]. For the preparation of SWCNT-RGO dispersion, SWCNT (30 mg) and PEDOT:PSS (30 mg) were added into 30 mL of water, followed by bath sonication for 1 h and tip sonication for 20 min to obtain a uniform SWCNT dispersion. RGO was also dispersed in water with a concentration

of 1 mg/mL in parallel. After that, SWCNT and RGO dispersion were mixed to obtain mixture with different contents of RGO (0, 5, 10, 30, 50, and 70 wt%).

Preparation of TPU/SWCNT-RGO/PU strain sensor

A solution of TPU (30 wt%) was prepared using DMF as the solvent under heating and stirring. The PU multifilament was immersed into the SWCNT-RGO dispersion for 2 s and subsequently dried at 60 °C. After repeating this process 15 times, the as-prepared SWCNT-RGO/PU core–sheath fiber was dipped into the TPU solution, immediately taken out, and dried to obtain the TPU/SWCNT-RGO/PU composite fiber. Finally, both ends of the fiber were connected with copper wires and fixed with label paper to obtain TPU/SWCNT-RGO/PU strain sensor.

Characterizations

The structure and morphology of the samples were observed by hot stage polarizing light microscopy (BX51-P, Japan), field emission scanning electron microscope (FESEM, S-4800, Japan), and transmission electron microscopy (TEM, JEM-2100F, Japan). To investigate the cross-sectional morphology, the samples were wrapped with epoxy resin, immersed in liquid nitrogen, and then fractured in liquid nitrogen. Subsequently, FESEM was employed to observe fracture surface of the samples. The washability measurement was conducted in an ultrasonic bath (SK1200H, China, ultrasonic power: 50 W). For sensor performance evaluation, the stretching speed was adjusted over different strain ranges to obtain a stable electrical signal. The current signal of the sensor was measured in real time by using a two-point measurement of the electrochemical workstation (Autolab PGSTAT204, Switzerland) and the copper clamp.

Results and discussion

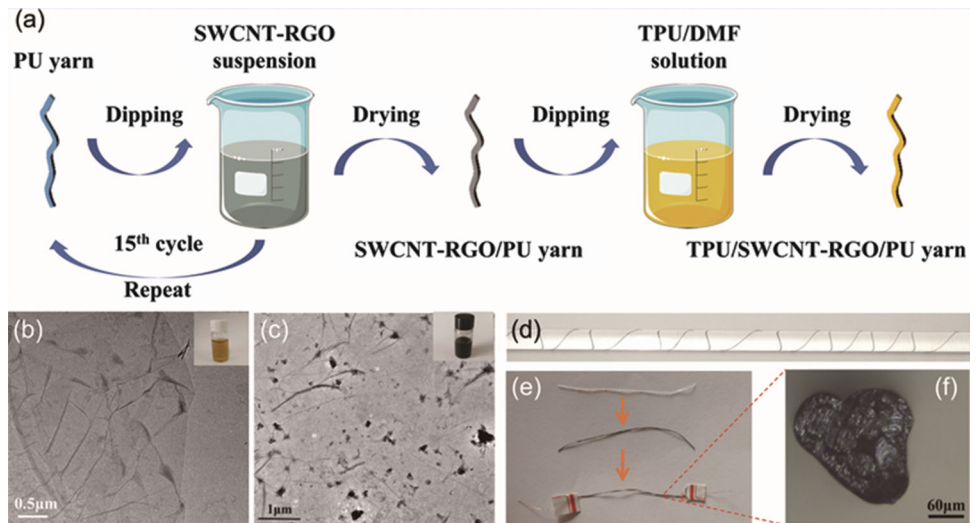
Preparation of TPU/SWCNT-RGO/PU strain sensor

As shown in Fig. 1a, the preparation of the TPU/SWCNT-RGO/PU composite fiber is mainly divided into two steps: SWCNT-RGO suspension was dip-

coated onto the elastic PU multifilament, and then, a TPU sheath was applied as a protective layer. First, we used PEDOT:PSS as a stabilizer, and RGO was prepared by reducing GO in hydrazine hydrate. TEM image shows the typical wrinkled and transparent appearance of RGO (Fig. 1b). Second, different volumes of SWCNT and RGO dispersion were mixed to obtain different concentrations of SWCNT and RGO with the PEDOT:PSS as a dispersant. This is due to the π - π interaction between the aromatic moieties of the PEDOT:PSS, RGO, and SWCNT, contributing to improved wetting and infiltration of the RGO and SWCNT agglomerates. The resulted lower interfacial tension is conducive for the well dispersion of conductive fillers. TEM image shows (Fig. 1c) that SWCNT are disassembled and homogeneously distributed on RGO, suggesting the efficient dispersion of SWCNT and RGO by PEDOT:PSS. By repeating the dip-coating of SWCNT-RGO on PU multifilament, a stable conductive layer was formed, resulting in the SWCNT-RGO/PU core–sheath fiber. Finally, TPU/SWCNT-RGO/PU strain sensor was fabricated by a quick dip of the as-prepared core–sheath fiber into the TPU solution and drying. As shown in Fig. 1d–f, the color of composite fiber changed from white to black, and finally bright black, suggesting the coating of conductive layer in fiber sensor.

The morphology of TPU/SWCNT-RGO/PU composite fiber was observed by using the SEM. In Fig. 2a and b, a multifilament structure of pure PU with a uniform diameter ($\sim 150 \mu\text{m}$) can be observed clearly. After dipping and drying, a tulle-like SWCNT-RGO conductive layer can be observed on the surface of the PU multifilament. (The content of RGO in conductive layer is 50 wt%.) In addition, after repeated dip-coating, the surface of the fiber composite is rough and dense (Fig. 2c and d), confirming a stable conductive layer was deposited. In contrast, after a quick dip into the TPU solution, a relatively smooth surface is shown in Fig. 2e and f, suggesting the successful formation of the TPU protective layer. In order to observe the structure of the composite fiber more clearly, we further investigated the cross-sectional morphology. Figure 2g and h shows an obvious sandwiched structure of the PU multifilament, SWCNT-RGO conductive layer, and the TPU protective layer (the outermost layer is epoxy resin). Meanwhile, the enlarged view manifests that the SWCNT-RGO layer ($\sim 0.75 \mu\text{m}$) was wrapped in the middle. During stretching, the presence of the

Figure 1 a Synthetic procedure of TPU/SWCNT-RGO/PU strain sensor. b TEM image of RGO. c TEM image of SWCNT-RGO with 50 wt% RGO. d Photograph of TPU/SWCNT-RGO/PU strain sensor. e Photographs of PU, SWCNT-RGO/PU, and TPU/SWCNT-RGO/PU strain sensor. f Cross-sectional optical micrograph of TPU/SWCNT-RGO/PU strain sensor.



protective layer could ensure the simultaneous deformation of the PU multifilament and SWCNT-RGO conductive layer, which makes the fiber sensor stable and durable. Due to the ultrathin characteristic of RGO, conductive layers with different weight ratios of RGO show similar morphologies.

Electromechanical performance of TPU/SWCNT-RGO/PU strain sensor

The mechanical and electrical properties of SWCNT-RGO/TPU strain sensor were studied in detail, as shown in Fig. 3. The uniaxial tensile speed was controlled at $5\% \text{ s}^{-1}$ to measure relative resistance change ($\Delta R/R_0$). Figure 3a shows that $\Delta R/R_0$ of strain sensors with different RGO weight ratios generally increased with the tensile strain. In contrast to TPU/SWCNT/PU sensor, with the increasing weight ratio of RGO, $\Delta R/R_0$ increases more significantly with the increasing strain. The sensing range of the strain sensor with 50 wt% and 70 wt% RGO can reach up to 465%, and $\Delta R/R_0$ at this point is, respectively, 269.9 and 471.8, which is much higher than that of the TPU/SWCNT/PU sensor ($\Delta R/R_0 = 46.4$). This is because the network of 1D SWCNT could maintain the interconnection under external strain, resulting in inconspicuous resistance change. The addition of 2D RGO into 1D SWCNT network could increase the contact area, which can be more effectively disrupted under strain and lead to more significant resistance change. As shown in Fig. 3b, three linear regions can be observed during the stretching process in fiber sensor with 50 wt% RGO in conductive layer: 1–

150%, 150–300%, and 300–465%. The corresponding GFs [$GF = (\Delta R/R_0)/\epsilon$] for these regions are 8.76, 43.8, and 114.7, respectively. In addition, the sensor exhibited GFs of 11.5, 57.7, and 215.0 in these strain regions with 70 wt% RGO in conductive layer (Fig. 3c). These data suggest that the sensibility is tunable by adjusting the concentration of RGO. In comparison, the GFs of TPU/SWCNT/PU sensor in these regions are just 2.1, 7.7, and 17.3, respectively, demonstrating the advantageous of RGO in improving the sensitivity of sensor. However, it is found that further increasing content of RGO would result in brittle fiber and limited sensing range.

To demonstrate the washability of TPU/SWCNT-RGO/PU strain sensor, both SWCNT-RGO/PU and TPU/SWCNT-RGO/PU composite fibers were placed in an ultrasonic bath (ultrasonic power: 50 W). The curves of $\Delta R/R_0$ versus time are plotted in Fig. 3d. Notably, with the TPU sheath, the $\Delta R/R_0$ of TPU/SWCNT-RGO/PU composite fiber only increased by 10 after ultrasonication for 60 min and then remained stable for the next 190 min. In contrast, the $\Delta R/R_0$ of the SWCNT-RGO/PU sensor increased significantly with increasing ultrasound time, and the $\Delta R/R_0$ even reached 690 at 60 min, which indicates the serious destruction of the conductive layer. Therefore, compared with SWCNT-RGO/PU sensor, the protective layer endows TPU/SWCNT-RGO/PU strain sensor with excellent stability in water, which is critical for wearable sensing textiles.

Notably, when the fiber was drawn to 350% with different strain rates, little difference in the $\Delta R/R_0$

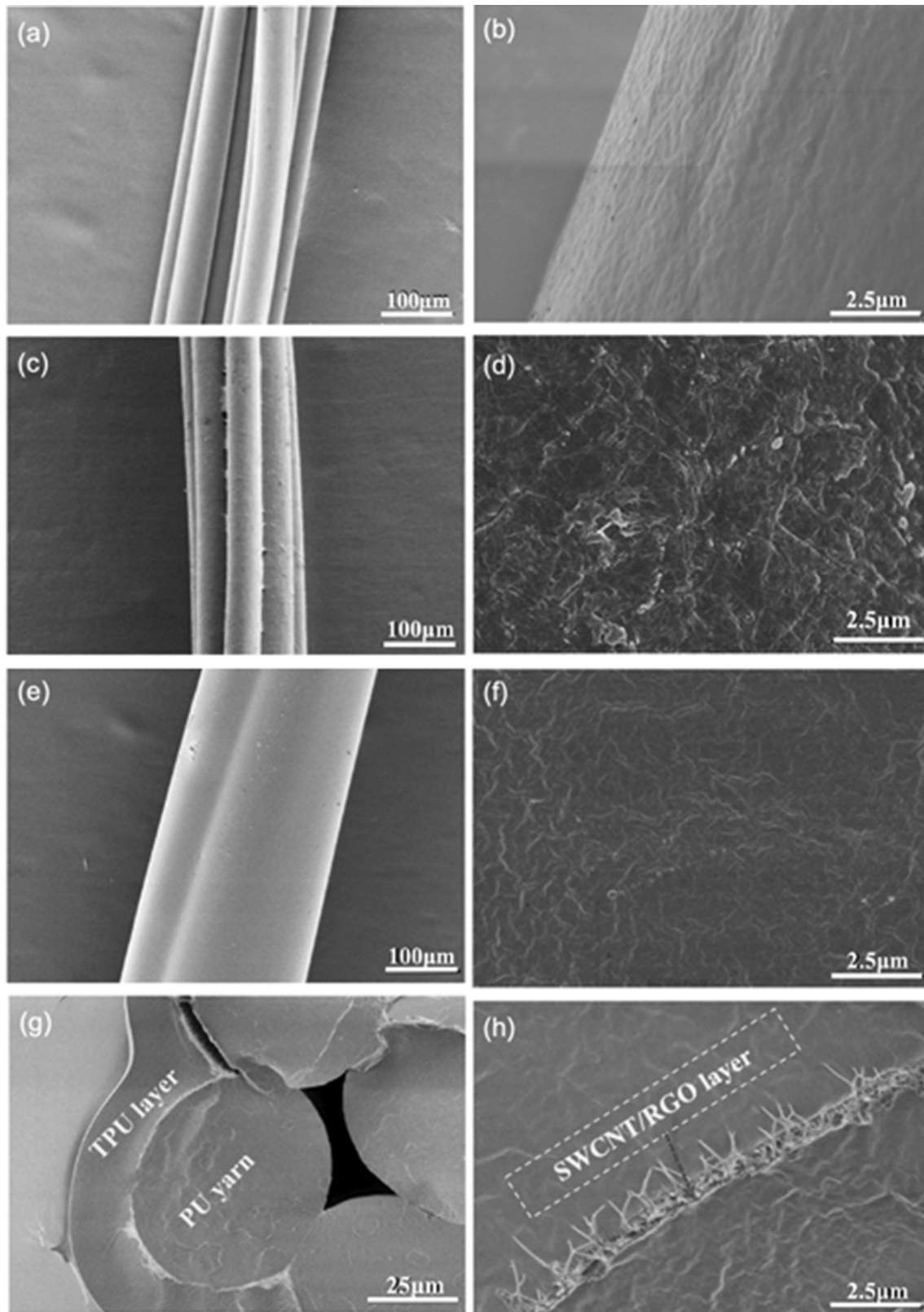


Figure 2 a, b SEM images of PU multifilament in different magnifications. c, d SEM images of SWCNT-RGO/PU fiber in different magnifications. e, f SEM images of TPU/SWCNT-RGO/

PU fiber in different magnifications. g, h Cross-sectional SEM images of TPU/SWCNT-RGO/PU fiber in different magnifications.

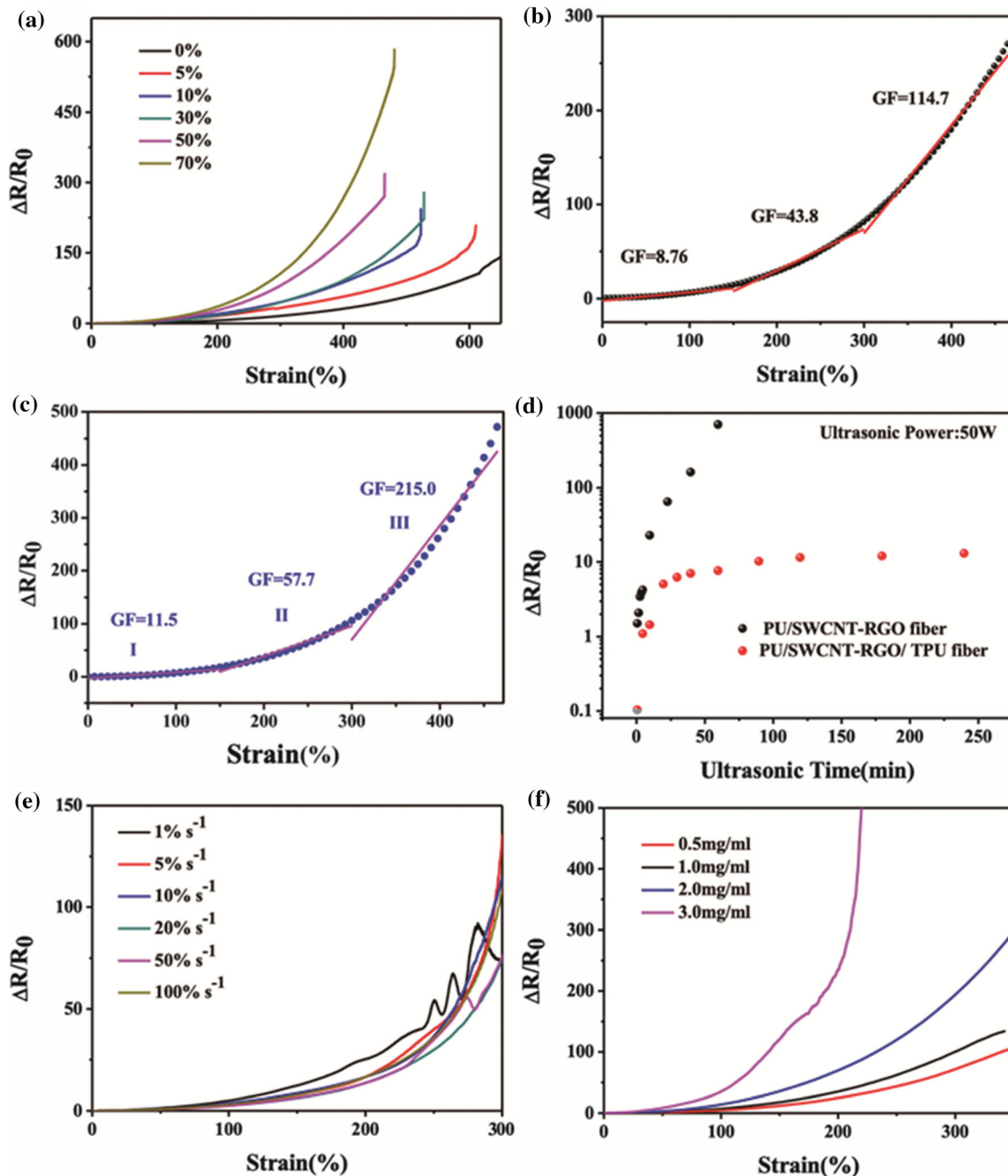


Figure 3 a $\Delta R/R_0$ of fiber strain sensors with different RGO contents as a function of applied strain. b $\Delta R/R_0$ and GF of the fiber strain sensor with 50 wt% RGO as a function of applied strain. c $\Delta R/R_0$ and GF of the fiber strain sensor with 70 wt% RGO as a function of applied strain. d $\Delta R/R_0$ of the fiber strain

sensor with 50 wt% RGO as a function of ultrasonic time. e $\Delta R/R_0$ of the fiber strain sensor with 50% RGO under different strain rates (1–100% s^{-1}) as a function of applied strain. f $\Delta R/R_0$ of fiber strain sensors with different amounts of conductive fillers as a function of applied strain.

change can be observed (Fig. 3e), indicating the high stability of our strain sensor, and its conductivity is not affected by the strain rate. However, the amount of conductive fillers has a significant impact on the electromechanical performance of strain sensors. In

general, higher $\Delta R/R_0$ was observed for the composite fiber with a larger amount of SWCNT-RGO (Fig. 3f). Notably, when the suspension concentration increased to 3 mg/ml, a higher $\Delta R/R_0$ of 379.9 can be attained, while resulting in a limited sensing range

from 0 to 216%. The trade-off relationship between the $\Delta R/R_0$ and stretchability of sensors can be attributed to the intrinsic rigidity of the inorganic component, which leads to plastic deformation under large strains. Or the result may be due to the inhomogeneous distribution of SWCNT-RGO in large concentrations. Therefore, strain sensors with different sensitivities and sensing ranges can also be fabricated by adjusting the concentration of SWCNT-RGO besides the weight ratio of SWCNT to RGO.

We further compared the sensitivity and stretchability of our strain sensor with other recently reported fiber sensors [2, 9, 28, 45–54]. As shown in Fig. 4, the core–sheath NTTF₅@fibers [54] have the largest working range (~ 1135%) among the selected reported strain sensors, but the GF is only 34.2. The CSF fiber sensor [46] shows the highest GF, but the working range limits to 330%. In addition, using the same dip-coating method, the sensing range of the spandex yarns coated graphene nanoplatelets (GnP) as a conductive filler is 104%, and the GF is only 13.2 [50]. Thus, achieving both high working strain and high GF is still a challenge as exemplified by these reported fiber sensors. In comparison with these fiber sensors, our TPU/SWCNT-RGO/PU strain sensor presents a combined high gauge factor of 114.7 and 215.0, and high maximum working strain of 465%, which is attribute to the combination of the synergistic effect of SWCNT and RGO and the encapsulation of TPU protective layer.

Hysteresis is an important factor for strain sensors under dynamic load, especially for wearable devices. Elastic recovery tests were thus carried out to evaluate the irreversible deformation. As shown in Fig. 5a, a similar hysteresis pattern was observed

regardless of strain range, and an obvious hysteresis phenomenon occurred when larger strains applied, indicating the rearrangement or even damage of the SWCNT-RGO network and the irreversible deformation of elastic TPU and PU substrates under large strains. In the repeating cycles of loading/unloading tests (Fig. 5b), both the mechanical hysteresis and stress softening decreased for the initial two cycles and remained stable for the next cycles, demonstrating the pretrained sensor has a high stability and elasticity, which can be attributed to the Mullins effect [39, 55, 56].

Furthermore, we demonstrated the stability and repeatability of TPU/SWCNT-RGO/PU strain sensor, by measuring the change of $\Delta R/R_0$ with repeated stretching–releasing cycles under different strains. Figure 6a and b shows the change of resistance of the sensor under a small strain of 1–50% and a larger strain of 100–300%, respectively. Apparently, under both small strains (10–50%) and relatively higher strains (100–300%), the $\Delta R/R_0$ remained stable with little changes. This phenomenon indicates that during the repeated stretching–releasing cycles under different strains, the conductive network sensitively broken and restored to build effective conduction paths, which contributed to the excellent flexibility and repeatability of TPU/SWCNT-RGO/PU strain sensor. The high durability of the strain sensor was further demonstrated with 1000 stretching–releasing cycles, as shown in Fig. 6c. The resistance increased at the initial 20 cycles and tended to be stable after several stretching–releasing cycles. This is attributed to the additional breakdown of the conductive network at the beginning and the stabilization of the network under repeated loading cycles [21]. The

Figure 4 Comparison of the maximum working range and maximum GF of recently reported fiber sensors.

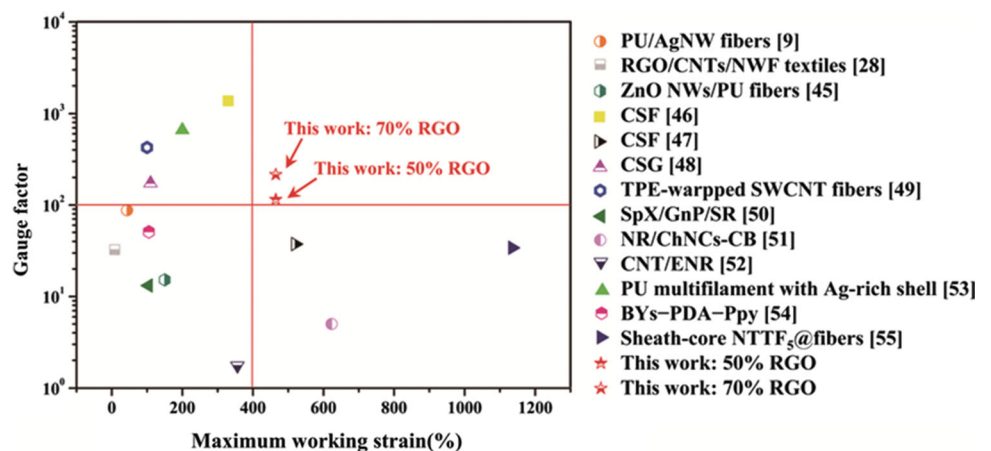


Figure 5 **a** Stretching–releasing stress–strain curves for the fiber strain sensor with 50 wt% RGO at strains of 10%, 20%, 30%, 40%, 50%, 100%, 200%, and 300%. **b** Stress–strain curves of initial five cycles of the fiber strain sensor at strains of 10%, 20%, 30%, 40%, 50%, 100%, 200%, and 300%.

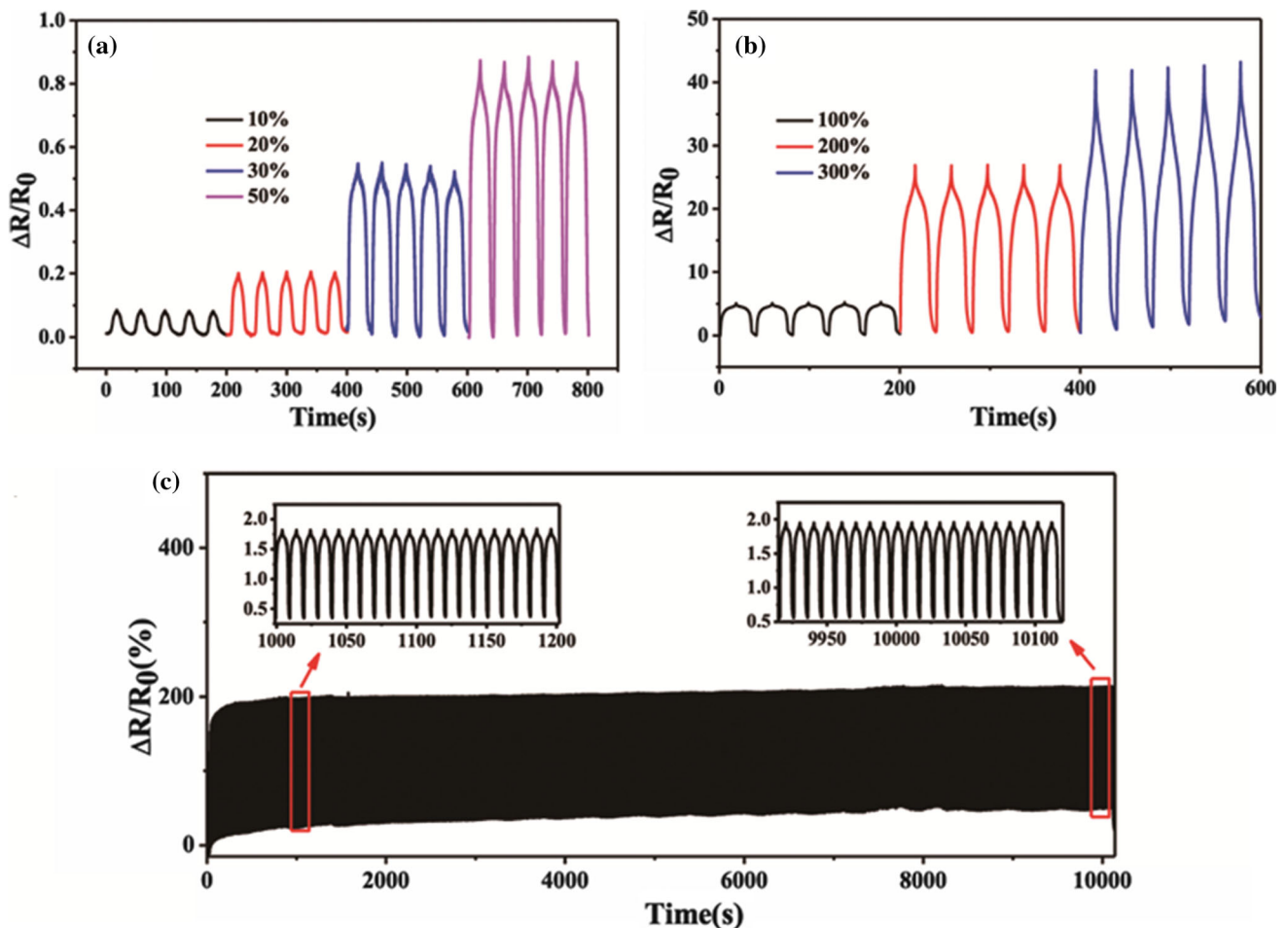
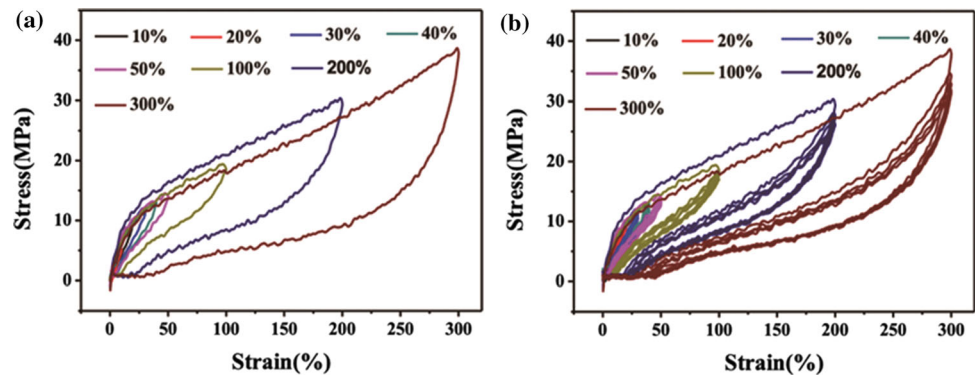


Figure 6 **a**, **b** $\Delta R/R_0$ of the fiber strain sensor in stretching–releasing cycles toward different strains. **c** $\Delta R/R_0$ of the fiber strain sensor in over 1000 stretching–releasing cycles toward a strain of

enlarged versions in Fig. 6c show that $\Delta R/R_0$ was stable in around 100 and 1000 cycles, revealing remarkable mechanical durability and repeatability of TPU/SWCNT-RGO/PU strain sensor.

In addition, we also monitored the surface morphology of the TPU/SWCNT-RGO/PU composite

50% and a strain rate of $10\% \text{ s}^{-1}$. The insets represent the sensing behaviors in 100–120 and 991–1013 cycles.

fiber under different strains (Fig. 7a). During the stretching process, besides the decreasing of the fiber diameter, no obvious change can be observed on the surface of the fiber, which indicates the TPU layer effectively protects the internal conductive layer from breaking or even flaking off under strains. In contrast,

obvious cracks exhibited on SWCNT-RGO/PU composite fiber without the protective layer, which gradually expanded with increasing strains (Fig. 7b). Furthermore, after stretching to 300%, obvious signs of flaking off can be observed on SWCNT-RGO/PU composite fiber. In addition, when the strain was unloaded, the cracks on the fiber cannot restore in SWCNT-RGO/PU fiber.

Applications of TPU/SWCNT-RGO/PU strain sensor

Due to the high sensitivity, wide sensing range, durability, and fibrous one-dimensional structure of TPU/SWCNT-RGO/PU strain sensor, it has great potential in wearable electronic devices. Figure 8a–g shows small human motions detected with the strain sensor. The as-prepared strain sensor (with 50 wt% RGO in conductive layer) was firstly adhered on to Adam's apple to monitor the vibration of the vocal cord, as shown in Fig. 8a. When the volunteer spoke

Figure 8 Monitoring of different human activities: a–c phonation when the volunteer pronounced different words “First,” “Second,” and “Carbon,” d neck bending, e fingers opening and closing, f wrist bending, g arteries pulse, h drinking water, and i click and double click of the mouse.

different words, such as “First,” “Second,” and “Carbon,” obvious differences can be distinguished from the response curves (Fig. 8b, c). To demonstrate the capability of monitoring the muscle movements, the strain sensor was further placed on the neck, finger, and wrist. As shown in Fig. 8d–f, obvious current fluctuation can be observed when the volunteer was looking down, opening and closing fingers or bending the wrist. Notably, when the sensor was firmly fixed to the arteries, subtle current fluctuations can be observed, indicating the potential of the sensors in the real-time monitor of the pulse (Fig. 8g). Based on this result, an intelligent wearable device can be developed for continuous health

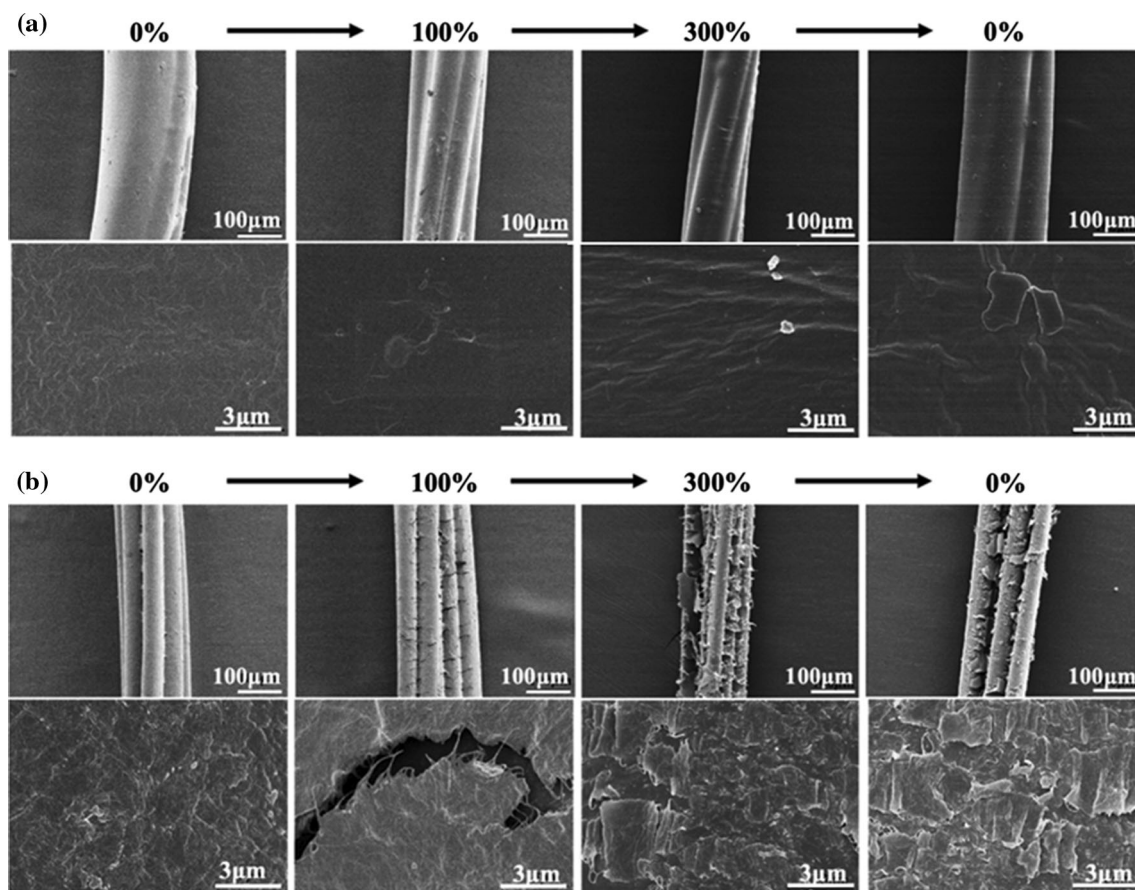
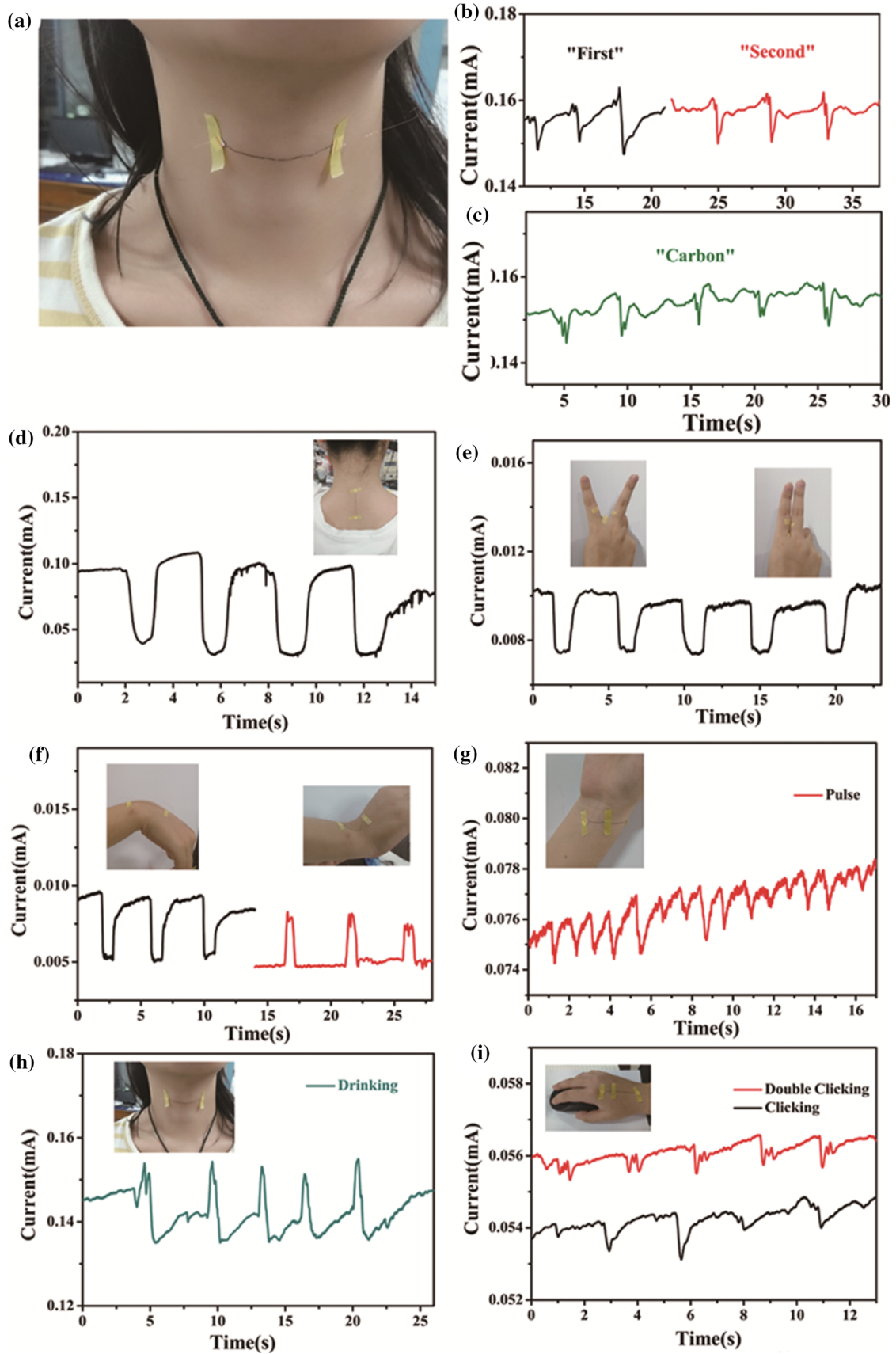


Figure 7 SEM images of **a** TPU/SWCNT-RGO/PU fiber and **b** SWCNT-RGO/PU fiber under a stretching–releasing cycle ($\varepsilon = 0\text{--}300\%$) in different magnifications.



monitor, revealing timely information on the state of the human body. In addition, the sensor can be used for monitoring the behavior of drinking water (Fig. 8h). Moreover, from the frequency and magnitude of the signal caused by the sensor attached to the hand, the click and double click of the mouse can be monitored (Fig. 8i).

Apart from small motions, our sensor is able to detect large body movements due to the high working strain. As shown in Fig. 9a and b, when bending the elbow, the lower muscle stretched and the upper muscle contracted; thus, different current fluctuations were generated to distinguish these two motions. Similarly, it is easy to recognize movements during walking and jumping with different current changes (Fig. 9c).

It is interesting to note that our strain sensor can be used to detect strains underwater. For example, we attached the sensor on a balloon and pressed the balloon in water, as shown in Fig. 9d. The current mode indicates that our sensor is able to accomplish

underwater work. It is worth noting that the outstanding underwater work performance of the sensor is achieved by coating the TPU protective layer. These results reveal that TPU/SWCNT-RGO/PU strain sensor shows great potential for smart wearable systems, textile electronics, and stretchable electronics.

Conclusion

In summary, using the PU multifilament as a scaffold, SWCNT-RGO as the conductive layer, and TPU as a protective layer, we have developed a simple, cost-effective, and scalable method to fabricate fiber strain sensors with high sensitivity, wide sensing range, durability, and flexibility. The sensor featured a wide sensing range of up to 465%, a high GF of 114.7 at 465% strain, and good cyclic stability for over 1000 stretching cycles. In addition, by adjusting the RGO addition to 70 wt%, a higher gauge factor of

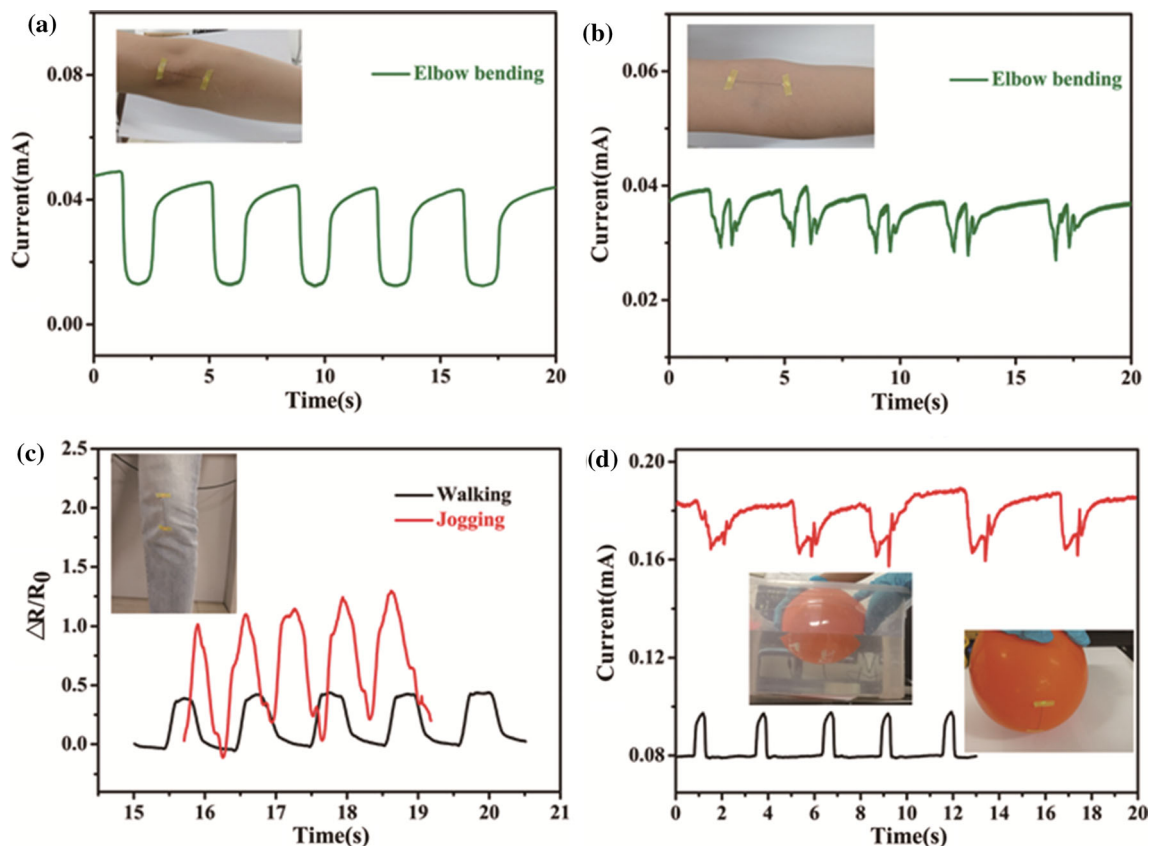


Figure 9 Detection of large body movements using the fiber strain sensors. Response to the motions of **a**, **b** wrist bending (up and down) and **c** walking and jogging. **d** Monitoring of pressing the

balloon underwater; the insert is the photograph of the fiber strain sensor attached on an expanded balloon.

215.0 at the same strain can be attained. The experimental observations indicated that the synergistic effect between SWCNTs and RGO contributes to the formation of effective conductive networks and results in the high sensitivity of the strain sensor. In addition, the TPU sheath enables the fiber strain sensor with outstanding durability and excellent underwater work performance. We demonstrated that TPU/SWCNT-RGO/PU strain sensor is greatly promising for wearable electronics by the monitor of various human movements from tiny motions like pulse to large motions like jumping and running. Moreover, the fiber strain sensor can even perform underwater detection. Based on the high performance of our fiber strain sensor, we believe that it paves a new way to next-generation intelligent wearable technology.

Funding

This study was funded by the Natural Science Foundation of Shanghai (Grant No. 17ZR1401100) and the Fundamental Research Funds for the Central Universities (Grant No. 2232019D3-01).

Compliance with ethical standards

Conflict of interest The authors declare that they have no conflict of interest.

References

- [1] Amjadi M, Kyung K, Park I, Sitti M (2016) Stretchable, skin-mountable, and wearable strain sensors and their potential applications: a review. *Adv Funct Mater* 26:1678–1698. <https://doi.org/10.1002/adfm.201504755>
- [2] Lee J, Shin S, Lee S, Song J, Kang S, Han H, Kim S, Kim S, Seo J, Kim D, Lee T (2018) Highly sensitive multifilament fiber strain sensors with ultrabroad sensing range for textile electronics. *ACS Nano* 12:4259–4268. <https://doi.org/10.1021/acsnano.7b07795>
- [3] Meng Q, Wu H, Mao L, Yuan H, Ahmad A, Wei Z (2017) Combining electrode flexibility and wave-like device architecture for highly flexible Li-ion batteries. *Adv Mater Technol* 2:1–7. <https://doi.org/10.1002/admt.201700032>
- [4] Wang L, Zhang Y, Pan J, Peng H (2016) Stretchable lithium-air batteries for wearable electronics. *J Mater Chem A* 4:13419–13424. <https://doi.org/10.1039/c6ta05800k>
- [5] Kim H, Yoon J, Lee G, Paik S, Choi G, Kim D, Kim B, Zi G, Ha J (2016) Encapsulated, high-performance, stretchable array of stacked planar micro-supercapacitors as waterproof wearable energy storage devices. *ACS Appl Mater Interfaces* 8:16016–16025. <https://doi.org/10.1021/acsami.6b03504>
- [6] Li X, Wang J, Zhao Y, Ge F, Komarneni S, Cai Z (2016) Wearable solid-state supercapacitors operating at high working voltage with a flexible nanocomposite electrode. *ACS Appl Mater Interfaces* 8:25905–25914. <https://doi.org/10.1021/acsami.6b06156>
- [7] Lee S, Choi K, Kim S, Lee S (2018) Wearable supercapacitors printed on garments. *Adv Funct Mater* 28:1–10. <https://doi.org/10.1002/adfm.201705571>
- [8] Wang X, Sun H, Yue X, Yu Y, Zheng G, Dai K, Liu C, Shen C (2018) A highly stretchable carbon nanotubes/thermoplastic polyurethane fiber-shaped strain sensor with porous structure for human motion monitoring. *Compos Sci Technol* 168:126–132. <https://doi.org/10.1016/j.compscitech.2018.09.006>
- [9] Zhu G, Ren P, Guo H, Jin Y, Yan D, Li Z (2019) Highly sensitive and stretchable polyurethane fiber strain sensors with embedded silver nanowires. *ACS Appl Mater Interfaces* 11:23649–23658. <https://doi.org/10.1021/acsami.9b08611>
- [10] Wang Z, Huang Y, Sun J, Huang Y, Hu H, Jiang R, Gai W, Li G, Zhi C (2016) Polyurethane/cotton/carbon nanotubes core-spun yarn as high reliability stretchable strain sensor for human motion detection. *ACS Appl Mater Interfaces* 8:24837–24843. <https://doi.org/10.1021/acsami.6b08207>
- [11] Ma L, Yang W, Wang Y, Chen H, Xing Y, Wang J (2018) Multi-dimensional strain sensor based on carbon nanotube film with aligned conductive networks. *Compos Sci Technol* 165:190–197. <https://doi.org/10.1016/j.compscitech.2018.06.030>
- [12] Liu Q, Zhang M, Huang L, Li Y, Chen J, Li C, Shi G (2015) High-quality graphene ribbons prepared from graphene oxide hydrogels and their application for strain sensors. *ACS Nano* 9:12320–12326. <https://doi.org/10.1021/acsnano.5b05609>
- [13] Yin B, Wen Y, Hong T, Xie Z, Yuan G, Ji Q (2017) Highly stretchable, ultrasensitive, and wearable strain sensors based on facilely prepared reduced graphene oxide woven fabrics in an ethanol flame. *ACS Appl Mater Interfaces* 9:32054–32064. <https://doi.org/10.1021/acsami.7b09652>
- [14] Karim N, Afroj S, Tan S, Pei He, Fernando A, Carr C, Novoselov K (2017) Scalable production of graphene-based wearable E-textiles. *ACS Nano* 11:12266–12275. <https://doi.org/10.1021/acsnano.7b05921>
- [15] Meng Q, Liu Z, Han S, Xu L, Araby S, Cai R, Zhao Y, Lu S, Liu T (2019) A facile approach to fabricate highly sensitive, flexible strain sensor based on elastomeric/graphene platelet

- composite film. *J Mater Sci* 54:10856–10870. <https://doi.org/10.1007/s10853-019-03650-1>
- [16] Wu X, Han Y, Zhang X, Zhou Z, Lu C (2016) Large-area compliant, low-cost, and versatile pressure-sensing platform based on microcrack-designed carbon black@polyurethane sponge for human-machine interfacing. *Adv Funct Mater* 26:6246–6256. <https://doi.org/10.1002/adfm.201601995>
- [17] Chen Y, Wang L, Wu Z, Luo J, Li B, Huang X, Xue H, Gao J (2019) Super-hydrophobic, durable and cost-effective carbon black/rubber composites for high performance strain sensors. *Compos Part B Eng* 176:107358. <https://doi.org/10.1016/j.compositesb.2019.107358>
- [18] Shin M, Lee B, Kim S, Lee J, Spinks G, Gambhir S, Wallace G, Kozlov M, Baughman R, Kim S (2012) Synergistic toughening of composite fibres by self-alignment of reduced graphene oxide and carbon nanotubes. *Nat Commun* 3:650. <https://doi.org/10.1038/ncomms1661>
- [19] Li L, Xu L, Ding W, Lu H, Zhang C, Liu T (2019) Molecular-engineered hybrid carbon nanofillers for thermoplastic polyurethane nanocomposites with high mechanical strength and toughness. *Compos Part B Eng* 177:107381. <https://doi.org/10.1016/j.compositesb.2019.107381>
- [20] Yang Y, Shi L, Cao Z, Wang R, Sun J (2019) Strain sensors with a high sensitivity and a wide sensing range based on a $Ti_3C_2T_x$ (MXene) nanoparticle-nanosheet hybrid network. *Adv Funct Mater* 29:1807882. <https://doi.org/10.1002/adfm.201807882>
- [21] Liu H, Gao J, Huang W, Dai K, Zheng G, Liu C, Shen C, Yan X, Guo J, Guo Z (2016) Electrically conductive strain sensing polyurethane nanocomposites with synergistic carbon nanotubes and graphene bifillers. *Nanoscale* 8:12977–12989. <https://doi.org/10.1039/C6NR02216B>
- [22] Zheng Y, Li Y, Dai K, Wang Y, Zheng G, Liu C, Shen C (2018) A highly stretchable and stable strain sensor based on hybrid carbon nanofillers/polydimethylsiloxane conductive composites for large human motions monitoring. *Compos Sci Technol* 156:276–286. <https://doi.org/10.1016/j.compscitech.2018.01.019>
- [23] Yang H, Gong L, Zheng Z, Yao X (2020) Highly stretchable and sensitive conductive rubber composites with tunable piezoresistivity for motion detection and flexible electrodes. *Carbon* 158:893–903. <https://doi.org/10.1016/j.carbon.2019.11.079>
- [24] Shi J, Hu J, Dai Z, Zhao W, Liu P, Zhao L, Guo Y, Yang T, Zou L, Jiang K, Li H, Fang Y (2017) Graphene welded carbon nanotube crossbars for biaxial strain sensors. *Carbon* 123:786–793. <https://doi.org/10.1016/j.carbon.2017.08.006>
- [25] Huang J, Her S, Yang X, Zhi M (2018) Synthesis and characterization of multi-walled carbon nanotube/graphene nanoplatelet hybrid film for flexible strain sensors. *Nano-materials* 8:786. <https://doi.org/10.3390/nano8100786>
- [26] Kim S, Song W, Yi Y, Min B, Mondal S, An K, Choi C (2018) High durability and waterproofing rGO/SWCNT-fabric-based multifunctional sensors for human-motion detection. *ACS Appl Mater Interfaces* 10:3921–3928. <https://doi.org/10.1021/acsami.7b15386>
- [27] Zhang F, Wu S, Peng S, Sha Z, Wang C (2019) Synergism of binary carbon nanofibres and graphene nanoplates in improving sensitivity and stability of stretchable strain sensors. *Compos Sci Technol* 172:7–16. <https://doi.org/10.1016/j.compscitech.2018.12.031>
- [28] Tang Z, Yao D, Du D, Ouyang J (2020) Highly machine-washable e-textiles with high strain sensitivity and high thermal conduction. *J Mater Chem C* 8:2741–2748. <https://doi.org/10.1039/C9TC06155J>
- [29] Amjadi M, Pichitpajongkit A, Lee S, Ryu S, Park I (2014) Highly stretchable and sensitive strain sensor based on silver nanowire-elastomer nanocomposite. *ACS Nano* 8:5154–5163. <https://doi.org/10.1021/nm501204t>
- [30] Tang D, Wang Q, Wang Z, Liu Q, Zhang B, He D, Wu Z, Mu S (2018) Highly sensitive wearable sensor based on a flexible multi-layer graphene film antenna. *Sci Bull* 63:574–579. <https://doi.org/10.1016/j.scib.2018.03.014>
- [31] Chen L, Weng M, Zhou P, Huang F, Liu C, Fan S, Zhang W (2019) Graphene-based actuator with integrated-sensing function. *Adv Funct Mater* 29:1–9. <https://doi.org/10.1002/adfm.201806057>
- [32] Chen J, Zhu Y, Jiang W (2020) A stretchable and transparent strain sensor based on sandwich-like PDMS/CNTs/PDMS composite containing an ultrathin conductive CNT layer. *Compos Sci Technol* 186:107938. <https://doi.org/10.1016/j.compscitech.2019.107938>
- [33] Lee H, Glasper M, Li X, Nychka J, Batcheller J, Chung H, Chen Y (2018) Preparation of fabric strain sensor based on graphene for human motion monitoring. *J Mater Sci* 53:9026–9033. <https://doi.org/10.1007/s10853-018-2194-7>
- [34] Park T, Yu S, Koo M, Kim H, Kim E, Park J, Ok B, Kim B, Noh S, Park C, Kim E, Koo C, Park C (2019) Shape-adaptable 2D titanium carbide (MXene) heater. *ACS Nano* 13:6835–6844. <https://doi.org/10.1021/acsnano.9b01602>
- [35] Zhao K, Niu W, Zhang S (2020) Highly stretchable, breathable and negative resistance variation textile strain sensor with excellent mechanical stability for wearable electronics. *J Mater Sci* 55:2439–2453. <https://doi.org/10.1007/s10853-019-04189-x>
- [36] Wu R, Ma L, Patil A, Meng Z, Liu S, Hou C, Zhang Y, Yu W, Guo W, Liu X (2020) Graphene decorated carbonized cellulose fabric for physiological signal monitoring and

- energy harvesting. *J Mater Chem A* 8:12665–12673. <https://doi.org/10.1039/D0TA02221G>
- [37] Yun Y, Hong W, Kim W, Jun Y, Kim B (2013) A novel method for applying reduced graphene oxide directly to electronic textiles from yarns to fabrics. *Adv Mater* 25:5701–5705. <https://doi.org/10.1002/adma.201303225>
- [38] Jeon J, Cho S, Jeong Y, Shin D, Kim N, Yun Y, Kim H, Choi S, Hong W, Kim H, Jin H, Kim B (2017) Pyroprotein-based electronic textiles with high stability. *Adv Mater* 29:1605479. <https://doi.org/10.1002/adma.201605479>
- [39] Ren M, Zhou Y, Wang Y, Zheng G, Dai K, Liu C, Shen C (2019) Highly stretchable and durable strain sensor based on carbon nanotubes decorated thermoplastic polyurethane fibrous network with aligned wave-like structure. *Chem Eng J* 360:762–777. <https://doi.org/10.1016/j.cej.2018.12.025>
- [40] Wang L, Tian M, Zhang Y, Sun F, Qi X, Liu Y, Qu L (2020) Helical core-sheath elastic yarn-based dual strain/humidity sensors with MXene sensing layer. *J Mater Sci* 55:6187–6194. <https://doi.org/10.1007/s10853-020-04425-9>
- [41] Cai G, Yang M, Pan J, Cheng D, Xia Z, Wang X, Tang B (2018) Large-scale production of highly stretchable CNT/cotton/spandex composite yarn for wearable applications. *ACS Appl Mater Interfaces* 10:32726–32735. <https://doi.org/10.1021/acsami.8b11885>
- [42] Afroj S, Karim N, Wang Z, Tan S, He P, Holwill M, Ghazaryan D, Fernando A, Novoselov K (2019) Engineering graphene flakes for wearable textile sensors via highly scalable and ultrafast yarn dyeing technique. *ACS Nano* 13:3847–3857. <https://doi.org/10.1021/acsnano.9b00319>
- [43] Yang Z, Pang Y, Han X, Yang Y, Ling J, Jian M, Zhang Y, Yang Y, Ren T (2018) Graphene textile strain sensor with negative resistance variation for human motion detection. *ACS Nano* 12:9134–9141. <https://doi.org/10.1021/acsnano.8b03391>
- [44] Xie X, Huang H, Zhu J, Yu J, Wang Y, Hu Z (2020) A spirally layered carbon nanotube-graphene/polyurethane composite yarn for highly sensitive and stretchable strain sensor. *Compos Part A Appl Sci Manuf* 135:105932. <https://doi.org/10.1016/j.compositesa.2020.105932>
- [45] Liao X, Liao Q, Zhang Z, Yan X, Liang Q, Wang Q, Li M, Zhang Y (2016) A highly stretchable ZnO@fiber-based multifunctional nanosensor for strain/temperature/UV detection. *Adv Funct Mater* 26:3074–3081. <https://doi.org/10.1002/adfm.201505223>
- [46] Tang Z, Jia S, Wang F, Bian C, Chen Y, Wang Y, Li B (2018) Highly stretchable core-sheath fibers via wet-spinning for wearable strain sensors. *ACS Appl Mater Interfaces* 10:6624–6635. <https://doi.org/10.1021/acsami.7b18677>
- [47] Wang C, Li X, Gao E, Jian M, Xia K, Wang Q, Xu Z, Ren T, Zhang Y (2016) Carbonized silk fabric for ultrastretchable, highly sensitive, and wearable strain sensors. *Adv Mater* 28:6640–6648. <https://doi.org/10.1002/adma.201601572>
- [48] Wang C, Xia K, Jian M, Wang H, Zhang M, Zhang Y (2017) Carbonized silk georgette as an ultrasensitive wearable strain sensor for full-range human activity monitoring. *J Mater Chem C* 5:7604–7611. <https://doi.org/10.1039/c7tc01962a>
- [49] Zhou J, Xu X, Xin Y, Lubineau G (2018) Coaxial thermo-plastic elastomer-wrapped carbon nanotube fibers for deformable and wearable strain sensors. *Adv Funct Mater* 28:1–8. <https://doi.org/10.1002/adfm.201705591>
- [50] Montazerian H, Rashidi A, Dalili A, Najjaran H, Milani A, Hoorfar M (2019) Graphene-coated spandex sensors embedded into silicone sheath for composites health monitoring and wearable applications. *Small* 15:1804991. <https://doi.org/10.1002/sml.201804991>
- [51] Liu Y, Wu F, Zhao X, Liu M (2018) High-performance strain sensors based on spirally structured composites with carbon black, chitin nanocrystals, and natural rubber. *ACS Sustain Chem Eng* 6:10595–10605. <https://doi.org/10.1021/acssuscemeng.8b01933>
- [52] Wu X, Han Y, Zhang X, Lu C (2017) Spirally structured conductive composites for highly stretchable, robust conductors and sensors. *ACS Appl Mater Interfaces* 9:23007–23016. <https://doi.org/10.1021/acsami.7b06256>
- [53] Pan J, Yang M, Luo L, Xu A, Tang B, Cheng D, Cai G, Wang X (2019) Stretchable and highly sensitive braided composite yarn@polydopamine@polypyrrole for wearable applications. *ACS Appl Mater Interfaces* 11:7338–7348. <https://doi.org/10.1021/acsami.8b18823>
- [54] Li L, Xiang H, Xiong Y, Zhao H, Bai Y, Wang S, Sun F, Hao M, Liu L, Li T, Peng Z, Xu J, Zhang T (2018) Ultrastretchable fiber sensor with high sensitivity in whole workable range for wearable electronics and implantable medicine. *Adv Sci* 5:1800558. <https://doi.org/10.1002/advs.201800558>
- [55] Lion A (1996) A constitutive model for carbon black filled rubber: Experimental investigations and mathematical representation. *Contin Mech Thermodyn* 8:153–169. <https://doi.org/10.1007/BF01181853>
- [56] Liu C, Choi J (2010) Strain-dependent resistance of PDMS and carbon nanotubes composite microstructures. *IEEE Trans Nanotechnol* 9:590–595. <https://doi.org/10.1109/TNAANO.2010.2060350>

Publisher's Note Springer Nature remains neutral with regard to jurisdictional claims in published maps and institutional affiliations.